Published in final edited form as:
Adv Healthc Mater. 2017 August ; 6(15): . doi:10.1002/adhm.201601462.

Control of Cell Alignment and Morphology by Redesigning ECM-mimetic Nanotopography on Multilayer Membranes

Maria P. Sousa[#], **Dr. Sofia G. Caridade**[#], and **Prof. João F. Mano**[#,*]
3B's Research Group - Biomaterials, Biodegradables and Biomimetics, University of Minho, Headquarters of the European Institute of Excellence on Tissue Engineering and Regenerative Medicine, AvePark, 4806-909 Taipas, Guimarães, Portugal

ICVS/3B's – PT Government Associate Laboratory, Braga/Guimarães, Portugal

Abstract

Inspired by native extracellular matrix (ECM) together with the multilevel architecture observed in nature, we engineer a material which topography recapitulates topographic features of the ECM and the internal architecture mimics the biological materials organization. The nanopatterned design along the XY plane is combined with a nanostructured organization along the Z axis on freestanding membranes prepared by layer-by-layer deposition of chitosan and chondroitin sulfate. Cellular behavior is monitored using two different mammalian cell lines, fibroblasts (L929) and myoblasts (C2C12), in order to perceive the response to topography. Viability, proliferation and morphology of L929 are sensitively controlled by topography; also differentiation of C2C12 into myotubes is influenced by the presence of nanogrooves. This kind of nanopatterned structure has been also associated with strong cellular alignment. To the best of our knowledge, it is the first time that such a straightforward and inexpensive strategy is proposed to produce nanopatterned freestanding multilayer membranes. Controlling cellular alignment plays a critical role in many human tissues, such as muscles, nerves or blood vessels, so these membranes can be potentially useful in specific tissue regeneration strategies.

Keywords

layer-by-layer; polysaccharides; nanogrooved freestanding membranes; cell alignment; C2C12 differentiation

1 Introduction

Directing cellular behavior is essential for different physiological processes and a very important stage of tissue-material interactions. The design of a surface capable of recapitulating features occurring *in vivo* may benefit the development of promising tissue engineering strategies.[1] Native extracellular matrix (ECM) has a unique and complex structure, displaying well-defined features on its topography such as protein fibers, pores, ridges, grooves that can be found at both micro and nanoscale levels.[1b, 2] Tissues like

* jmano@ua.pt.
#Present address: CICECO – Aveiro Institute of Materials, Department of Chemistry, University of Aveiro, 3810-193 Aveiro, Portugal

Europe PMC Funders Author Manuscripts

bone or muscle present highly aligned multiscale structures that have inspired the development of nanoengineered material for tissue regeneration applications;[2a] for instance, well-aligned, long and parallel cylinders of collagen type-I are part of the cortical bone structure, being important for its mechanical properties.[3]

Both chemical and topographical surface patterning play a recognized role in the regulation of the cellular behavior, at both micro and nanoscale levels.[4] The mechanisms behind cell response to nanotopographic features are more complex than the ones behind cellular response to microtopography, where cells are of comparable size to the features. In fact, the connection established between each cell and their environment is even observed at the nanoscale length.[1b] The cell surface receptors, particularly integrins, bind to the extracellular ligands and react to extracellular stimuli, including pattern motifs on the material's surface, inducing an intracellular cascade of physical and chemical events, conditioning cell response.[5] In particular, the geometry of topographical nanofeatures direct cells to react in terms of adhesion [6], formation of focal adhesions (FAs) [7], proliferation [8], migration [9], alignment [4a, 10] and differentiation [11]. For example, the surface topography of human cornea basement membrane was reproduced using lithography, inducing elongation and alignment of cells along the grooves.[12] Curiously when changing cell environment parameters like the growth medium, the cells reacted totally differently, suggesting that the patterning effect is also dependent of other environmental factors.[13] It was also found that both shape and alignment of mesenchymal stem cells is dependent on the nanotopographical density of the surface, regulating their function and even osteo- or neurogenesis.[14]

Distinct technologies have permitted the introduction of nanofeatures over the surface of biomaterials, allowing an additional cellular control in medical devices and substrates for cell culturing. Among conventional techniques are colloidal lithography [15], polymer demixing [16] or even phase separation [17], which are usually easier, faster and cheaper than other technologies, but with less control over the geometry.[18] In order to increase this control, techniques such as electron-bean and photolithography [4c, 19] have been extensively reported; however, the high costs associated with the limitation in the chosen raw materials prompt the need of finding alternative nanofabrication technologies.

With this in mind, there exists a present need for a single step process that could surpass some of the drawbacks of the existing technologies. We propose a simple layer-by-layer (LbL) methodology that presents high versatility, precise control over the film construction and ability to process under physiological and ambient conditions.[20] Lithographic techniques were already combined with LbL strategies to generate patterned surfaces [21]; however, the inability to detach the LbL film from the anchored substrate and to create asymmetric membranes increased the need of substrate-free LbL patterned films. Immersing a low-surface free energy substrate sequentially and continuously into polyelectrolytes of opposite charges is possible to obtain a multilayer film that can be easily detached from the underlying substrate. This method was employed before to produce smooth freestanding (FS) membranes.[22]

Unlike other nanofabrication methodologies, LbL allows the incorporation of a wide range of materials, since synthetic to natural polymers [22–23], proteins [24], or even other bioactive molecules [25]. We hypothesize that the sequential deposition of nanolayers of polyelectrolytes during the LbL buildup could adapt to the nanoscale the geometrical features of textured templates, generating multilayer membranes with the replica of the patterns upon detachment. As polysaccharides present structural similarities with natural ECM, have biodegradable properties and are biocompatible [26], chitosan (CHT) and chondroitin sulfate (CS) were chosen in this work as polycation and polyanion, respectively, to produce natural-based nanopatterned FS membranes.

The effect of the nanogrooves on cellular function was investigated by assessing the morphology, elongation, alignment of fibroblasts and myoblasts and differentiation in the case of myoblasts.

2 Results and discussion

2.1 Polyelectrolyte multilayers construction

Quartz Crystal Microbalance with Dissipation (QCM-D) was used to monitor the variations on the deposition of the polyelectrolytes and the thickness of the film along the time - see Figure S1A. As expected, frequency variation (Δf) decreased with the injection of CHT and CS, and with the increasing number of layers; this confirmed that the polyelectrolytes mass was deposited on the surface of the gold piezoelectric crystal. A slight increase in Δf was observed for the washing steps, which corresponds to the desorption of the excess of polyelectrolyte mass. In the other hand, dissipation variation (ΔD) increased with the consecutive injections of CHT and CS, evidencing the viscoelastic nature of the deposited polymers. A Voigt model was used to fit the QCM-D data and to estimate the thickness variation as a function of the number of deposited layers - see Figure S1B. The results showed a linear growth of the polyelectrolyte multilayer film ($R^2 = 0.974$), composed by CHT and CS layers, being an indication that the polymers were adsorb along the multilayer during the depositions, contrarily to other systems already described in literature.[27]

Based on the same model and parameters used to obtain the thickness, parameters like viscosity and shear modulus were also estimated - see Figure S1C and S1D, respectively. These two parameters increased along the buildup of the film, which can be related with the viscoelastic behavior of the film.[28] Fitting parameters like shear modulus, viscosity and thickness gave important continuous data on multilayer film construction.

2.2 Fabrication of nanopatterned FS films

Flat and nanopatterned membranes were produced by repeating 300 times the cyclic depositions on CHT and CS solutions, using appropriate templates. The underlying substrates selected to produce flat and nanopatterned membranes were polypropylene (PP) sheets and optical media material, respectively. The membranes were further crosslinked with genipin, to improve their mechanical and biological performance. After drying, both crosslinked and non-crosslinked membranes were easily detached from the underlying substrates, with the help of a tweezer. In the end, four formulations were designed: flat FS

([CHT/CS]$_{300}$), flat crosslinked FS (CL [CHT/CS]$_{300}$), nanopatterned FS (PAT [CHT/CS]$_{300}$) and nanopatterned crosslinked FS (PAT CL [CHT/CS]$_{300}$).

2.3 Morphological, topographical and physical characterization of the FS membranes

2.3.1 Morphology—The FS [CHT/CS]$_{300}$ films were detachable, without visible damages, from the respective underlying substrates. Figures 1A and 1B represent Scanning Electron Microscopy (SEM) micrographs of uncrosslinked and crosslinked flat FS membranes. Prior the crosslinking step, the membranes presented a homogeneous morphology with visible rough structures in the order of 1-2 μm. Crosslinked membranes showed a non-homogeneous morphology, with large and lower roughness areas randomly dispersed along the surface. The recordable part of the optical media presents nanofeatures on their surface.[29] We investigated the presence of this kind of topography on commercial blank optical media. The polycarbonate template used to create the nanotopography showed regular nanostructured stripes (width around 637 ± 36.1 nm) - see Figure 1C. The depth of the nanogrooves presented on the surface of the polycarbonate template was also calculated through SEM imaging - see Figure 1D; just by tilting the surface at 60° we were able to estimate the depth of the grooves (depth around 244 ± 16.2 nm). The LbL methodology was applied above these substrates trying to mimic their topographical features. It was possible to confirm the presence of a nanogrooved topography on the surface of both uncrosslinked and crosslinked FS patterned CHT/CS membrane - see Figures 1E and 1F, respectively. The results prove that the geometrical features of the polycarbonate template were successfully replicated on the FS membranes. The existence of the groove in the Z axis was confirmed by leaning the samples to 60°; Figure 1G clearly shows a depth on the stripe structures. Therefore, by using daily-used objects, such as optical media, we propose a pioneering and unconventional nanofabrication strategy, by transposing the defined nanoscale geometries of such simple substrates onto FS membranes. Anene-Nzelu, C.G. [29] had previously described the use of optical media as substrates for cellular alignment, controlling cells morphology and differentiation through its ordered nanotopography; however, polycarbonate can promote some problems in biointegration. So far, for the best of our knowledge is the first time that such multifaceted technology is used to fabricate, through the repetition of a single step, ordered nanopatterned freestanding membranes.

Differences were found in the cross-section between flat and nanopatterned FS membranes – see Figures 1H and 1I, respectively. Flat membranes were considerably thicker (40.4 ± 0.93 μm) than nanopatterned membranes (9.9 ± 0.21 μm), with the same number of bilayers. Such differences can be related with the established interactions between the underlying substrate and the polyelectrolytes. Estimated thickness obtained using QCM-D data shows a linear growth of the film, so if a 300 bilayer film was constructed, it should be obtained a FS membrane with the thickness around 7.6 μm. Comparing the estimated thickness with real thicknesses, we can conclude that polyelectrolytes interactions with polycarbonate template is closest to those with the gold piezoelectric crystal.

2.3.2 Topography—The studies of the topography of different human tissues, like heart, nerve or muscle, have been useful for understanding the threshold of the patterns dimensions capable to influence the cellular response. For instance, materials nanoimprinted with depth

of 200 nm and width of 500 nm were developed and the interactions between neuron cells and these nanograftings promoted both neurite alignment [30] and bipolarity [31]. Nanogrooved substrates with 450 nm in groove/ridge width; 100 or even 350 nm in depth regulated the orientation of cardiomyocytes and their contractile function.[32] As discussed below, our methodology provided such kind of dimensions, but using a quite simple methodology, providing the ability to use natural based polymers, employing wet based fabrication technologies.

Firstly, uncrosslinked and crosslinked flat FS membranes were analyzed with Atomic Force Microscopy (AFM) imaging - see Figure 2A and 2B respectively. Both presented some rough structures in the order of about 30 nm. Also the topography of the uncrosslinked and crosslinked nanopatterned FS films was investigated. AFM imaging confirmed the good reproducibility of the nanopatterning, always with structures consistent with the patterning of the polycarbonate template - see Figure 2C and 2D, respectively. Besides the presence of the sub-micron patterning, the topography of these surfaces also presented rough areas, at the nanometer scale. AFM was also performed with wet samples, in order to conclude about the stability of the patterning in a hydrated environment. As observed in Figure 2E and 2F, even after the incubation in phosphate buffered saline (PBS) overnight, the uncrosslinked and crosslinked nanopatterned surfaces maintained the nanogrooved topography. To conclude about the stability of patterning, we also left the membranes immersed in the PBS solution for longer times and even after 14 days we verify the maintenance of the patterning. This information will be further supported by the SEM images of the cells above the patterned freestanding membranes.

Figure 2G shows the arithmetic roughness (R_a) and the average height (H_{av}) values for all type of developed FS membranes. No substantially changes were observed with the crosslinking step, but the R_a value was slightly lower for the PAT CL $[CHT/CS]_{300}$ when comparing with the unmodified nanopatterned ones; this can be related with the swelling and contraction of the upper layer. Naturally, crosslinked and non-crosslinked PAT $[CHT/CS]_{300}$ presented significantly higher values of H_{av} due to the presence of the nanogrooves on their surface; indeed, the uncrosslinked patterned membranes clearly exhibited the highest value and this fact also can be related with the swelling process.

Some differences were expected when hydrating the membranes, due to their ability to retain water.[33] Figure 2H shows distinct relevant dimensions of the pattern features calculated through the AFM image data. The averaged ridge width (RW_{av}) in the FS films was similar between the different conditions, being around 500 nm. The averaged groove width (GW_{av}) was different, following what happened with the averaged depth (D_{av}) values: for PAT $[CHT/CS]_{300}$ membranes, the GW_{av} significantly decreased from 820.4 ± 40.7 nm (dry state) to 687.4 ± 64.1 nm (hydrated PAT $[CHT/CS]_{300}$). No significant differences in the GW_{av} were found between hydrated PAT CL $[CHT/CS]_{300}$ membranes and dried PAT CL $[CHT/CS]_{300}$; the crosslinking reaction allowed lower water contents in their composition and thus fewer differences were noticed in the GW_{av}. The D_{av} of the crosslinked and uncrosslinked FS membranes significantly increased when the samples were hydrated; in the case of PAT CL $[CHT/CS]_{300}$ the D_{av} significantly increased from 208.3 ± 38.36 nm (dry state) to 449.4 ± 50.01 nm (wet state). Curiously, in the hydrated state, crosslinked

membranes had higher values of depth than in the dry state. This is an indication that when hydrated, the topography of the PAT CL $[CHT/CS]_{300}$ membranes did not deform significantly along the XY plane but this changing essentially happened in the Z plane.

2.3.3 Water Contact Angle (WCA)—Wettability plays an important role in material-cell interactions;[34] it can depend on both chemical composition and topography of the surface. The WCA of the produced films are shown in Figure S2A and S2B. The crosslinking effect on the WCA was evident on flat CHT/CS membranes, with a significant increase on the hydrophilicity. The derivate of the crosslinking reaction is rich in hydrophilic groups, like amines, amides and hydroxyl groups;[35] indeed this result was consistent with some works in literature which reported the effect of genipin crosslinking in the decrease of the WCA, for hydrogels [36], capsules [35a] and also for multilayer films [37]. Significant differences were observed between flat and patterned membranes, for non-CL membranes (WCA = 107 ± 7.7°and WCA= 119 ± 3.1°, respectively) and for CL membranes (WCA = 74 ± 7.9°and WCA= 111 ± 1.3°, respectively). Therefore, the presence of a nanopatterned topography on the CHT/CS membranes enhanced the hydrophobicity of the surface, comparing with the flat ones. The explanation of this phenomenon is based on the Cassie-Baxter [38] regime that assumes that there is no penetration of the water droplets into the grooves, establishing a composite interface between the solid/air and the liquid droplet. In this case, if roughness increases, also the hydrophobicity of the surface will be higher, with higher WCA values. The effect of crosslinking was not significant in the case of patterned membranes, and we hypothesized that the crosslinking effect was masked by the patterning effect. Our results indicate that at this stage, surface topography prevented the decrease on WCA, that would be expectable by the introduction of hydrophilic groups. Similar competitive forces between hydrophilic surface groups and surface topography were already reported elsewhere.[39]

These results indicates that after an initial increase in hydrophobicity of glass surface with zeolite coverage, hydrophilic groups prevent the continuous increase in water contact angle with increasing zeolite density. In other words, the reason of the difference in the water contact angle values along the gradient surface can be attributed to the competitive effects between hydrophilic surface groups on zeolites and surface roughness.

2.3.4 Mechanical characterization of FS membranes—Dynamic Mechanical Analysis (DMA) experiments were performed to evaluate the mechanical/viscoelastic properties of the FS membranes. Mechanical studies are a vital part of the membranes characterization, as literature has been reported their determinant role on cellular phenotype and differentiation [40]. The variation of the storage (elastic) modulus (E') along the frequency is presented in Figure S3A. Overall, for all the studied FS membranes, E' slightly increases with frequency as already reported by other works.[41] Comparing the uncrosslinked membranes, it was observed that the curves of the graph were superimposed; thus, there are not significant differences in their E' values: 1.1 ± 0.40 MPa and 1.3 ± 0.32 MPa at 1 Hz, for unpatterned and patterned FS membranes, respectively. The same behavior was observed in the case of the crosslinked membranes where no significant differences could be found. However, significant differences were found between crosslinked and

uncrosslinked membranes, with *E'* values of the crosslinked FS membranes (4.3 ± 0.84 MPa and 4.4 ± 0.67 MPa at 1 Hz, for unpatterned and patterned crosslinked FS membranes, respectively) being higher than *E'* values of the uncrosslinked ones. Such results are consistent with previous works that reported an increase in stiffness when membranes were submitted to a crosslinked reaction.[37, 41a, 42] These results also indicate that the presence of the patterning or the polymeric nature of the template on both uncrosslinked and crosslinked FS membranes have not influence on the stiffness of the samples.

The variation of the loss factor (tan δ) along the frequency is presented in Figure S3B. The tan δ is the ratio of the amount of energy dissipated by viscous mechanisms relative to energy stored in the elastic component providing information about the damping properties of the membranes. For all membranes, it was observed that tan δ slightly increased with the frequency, but no signs of the presence of relaxation processes could be detected. Moreover, the uncrosslinked FS membranes presented higher dissipative properties, mainly at the higher frequencies.[43]

2.3.5 Degradation behavior monitoring of FS membranes—Both degradability and stability are important parameters in implantable scaffolds. Among other components, human serum presents enzymes capable to degrade biopolymers;[44] thus our developed membranes composed by CHT and CS can have interesting biodegradable properties. To understand the degradability of flat and nanopatterned CHT/CS, non-crosslinked and crosslinked, their weight loss was investigated, by immersing them in suitable enzymatic solutions. Lysozyme [45] and hyaluronidase [46] are enzymes capable to degrade natural polymers as CHT and CS once they are presented in the human serum at different concentrations. The degradation phenomenon could be noted through the decrease in the film thickness, as already reported in literature for comparable systems.[47] No substantial differences were observed in the weight loss profile between flat and patterned membranes - see Figure S4; nevertheless, the crosslink effect on the degradability and stability of the FS films was evident. The enzymatic degradation is retarded when the FS films were crosslinked. In fact, there are already some studies indicating the decrease of degradation rates for CL films and consequently the capability to use this strategy to control the material degradation.[47a, 48] Note that weight loss is also observed using just PBS solution, but it was accelerated with the presence of the enzymes. Looking deeper at Figure S4, it is possible to observe that most degradation occurs within the first 3 days of immersion; water molecules diffused into the bulk of the FS membranes, weakening their structure and thus enhancing the degradation. After 7 days of immersion the rate of degradation decreases significantly for FS membranes. The crosslinking effect can be used to control the degradation and thus the FS membranes characteristics may be adapted to the therapeutic specifications.

2.4 L929 cellular response

2.4.1 L929 viability and proliferation—We investigated the influence of the crosslinking and patterning in the FS membranes on the behavior of L929 cells. Figure 3A shows the results of a (3-(4,5-dimethylthiazol-2-yl)-5-(3-carboxymethoxyphenyl)-2-(4-sulfophenyl)-2H-tetrazolium) (MTS) assay, used to assess the mitochondrial redox activity.

One assumes that higher values of metabolic activity correspond to higher cellular viability. Differences between the non-crosslinked and crosslinked membranes became evident for day 3 and even more for day 7 of culture. In those time points, it was clearly observed higher values of cellular metabolic activity on crosslinked membranes. DNA quantification assay was used to complement these results and to have a measure of cell proliferation (see Figure 3B). Regarding the differences between non-crosslinked and crosslinked membranes, DNA quantification supported the results of MTS assay: in day 3 and day 7 of culture the crosslinked membranes induced significantly more proliferation. This fact matched with literature that has reported the positive effect of genipin on enhancing the cellular adhesion, viability and proliferation.[33, 36, 42] These works suggested that substrate stiffness increases when crosslinked with genipin, decreasing the water content and increasing the protein adsorption and resulting in improved cellular behavior. In fact, the mechanical properties of the membranes are also an important parameter to tailor the cellular behavior, and the crosslinking step with genipin seemed essential to increase the stiffness of the polysaccharide multilayer membranes and thus to enhance their biological performance, without compromising the non-cytotoxicity of the material. It can be said that the crosslinking effect on cell viability and proliferation followed the same trend along the days of culture but the same cannot be said for the effect of the topography. For day 7 of culture, the PAT CL $[CHT/CS]_{300}$ presented slightly higher DNA content and metabolic activity than flat CL $[CHT/CS]_{300}$ membranes while for uncrosslinked PAT $[CHT/CS]_{300}$ the DNA content and metabolic activity were slightly lower than for flat $[CHT/CS]_{300}$. We hypothesized that for CL membranes, the effect of genipin crosslinking overlapped the effect of topography. Literature [6, 49] reported the increasing number of filapodia and elongated cells when in presence of a nanogrooved surface, but this may not necessarily correspond to an increase in proliferation; other properties of the nanopatterned membranes can also play a role, such as surface chemistry, wettability or even stiffness. The influence of the presence of topography at nanoscale length on cellular proliferation can also depend on the cell type.[6, 50]

2.4.2 L929 morphology—A sparser density was chosen to culture fibroblasts, in order to avoid cell-cell contacts and to evidence the effect of topography on the morphology of individual cells. Fibroblasts were fixed and then stained to observe their nucleus and cytoskeleton variances on fluorescence microscopy - see Figure 4A. Cell morphology differed between flat and nanogrooved substrates. Overall, F-actin structure was different between fibroblasts adhered on flat and nanopatterned $[CHT/CS]_{300}$ membranes and fibroblasts were more elongated on the patterned ones, even for the first day of culture. On the other hand, differences on L929 morphology between non-CL and CL was also noted, mostly from the third day of culture; well-spread fibroblasts were observed on CL FS membranes. The effect of crosslinking on cell morphology was previously investigated in multilayers using high-throughput approaches, where the area occupied by L929 or SaOs-2 cells increased, as compared with uncrosslinked membranes.[51] Nevertheless, the topography seemed to have more impact on morphology and cytoskeleton organization than crosslink and stiffness. These findings are in accordance with previous studies; Yim *et al.* [7] stated that while both material nanotopography and stiffness are crucial properties to modulate mechanical properties of cells, nanotopography is the main property involved in

cytoskeletal organization and focal adhesions (FAs) formation. As observed for nanopatterned membranes, the cellular contact guidance followed a trend of orientation that was not observed for the flat ones. The first steps in the cellular contact guidance on nanogrooved surfaces is adhesion and guided spreading, with the cell usually assuming an elongated morphology parallel to the groove long axis;[52] the response changes according to parameters like geometry and respective dimensions of the nanotopographic features.

SEM analysis depicted the cells distribution over the flat and nanopatterned FS membranes - see representative images in Figure 4B for crosslinked membranes. The results obtained by fluorescence images (Figure 4A) were confirmed by SEM (Figure 4B); cell cultured over PAT CL $[CHT/CS]_{300}$ membranes presented predominantly a highly stretched morphology, aligned along the nanogrooves direction. As observed in Figure 4B, lamellipodia seemed to extend mostly towards the grooves and ridges direction (horizontally). However, when FAs were perpendicular to grooves direction, their limited width can be responsible for limiting the length of actin fibers and the random direction of lamellipodia. It was already reported that when lamellipodia are placed perpendicular to nanotopography direction, mesenchymal stem cells retract rapidly and become more round with dispersed filopodia.[53] Moreover, from Figure 4B we could also confirm the stability of the patterning on the surface of the membranes, even after 7 days of cell culture.

As already mentioned, there are different studies reporting the fabrication of nanopatterned materials and their respective topography-cells interactions but, for the best of our knowledge, this was the first time that nanopatterned FS membranes with ability to control cellular alignment, was fabricated by means of a single step process and using just natural-polymers.

2.4.3 Nuclei morphology—Although different investigations have already reported changes in the cytoskeleton morphology as a result of using a nanostructured topography, few studies have explored the differences in nuclear shape. Comparing the nuclei of the fibroblasts adhered on CL $[CHT/CS]_{300}$ and PAT CL $[CHT/CS]_{300}$ membranes, significant differences were found in terms of the nuclei elongation factor (EF) - see graphics in Figure S5A. When cultured on the patterned surface the nuclei of the cells predominantly showed an elliptical shape, while for unpatterned surfaces they preferred to display a circular shape, with no defined direction - see the representative images also presented in Figure S5A. Graphical distributions of the nucleus orientation of the individual cells cultured on unpatterned and patterned membranes during 1, 3 and 7 days of culture days are presented on Figure S5B. All the images were representative for each condition. On PAT CL $[CHT/CS]_{300}$ membranes, the larger part of nuclei was aligned in the same direction, with higher percentages of the cells between -10° and 10°, in opposite of what happened for CL $[CHT/CS]_{300}$ membranes. For unpatterned membranes, no significant differences were found in the range between -90° and 90°. These observations were according literature.[54]

2.4.4 Morphometric parameters—To have a quantitative idea of the nanotopography effect on cell (cytoskeleton) shape, we determined parameters like fibroblasts area, perimeter, circularity and alignment, regarding the third day of culture. Phalloidin-DAPI (4', 6-diamidino-2-phenylindole) stained images provided the ability to calculate parameters like

area and perimeter of the cells adhered on crosslinked flat and patterned $[CHT/CS]_{300}$ membranes - see Figure 5A. Flat surfaces exhibited a significantly larger cell area than patterned ones. If we assume that the volume of the cells will not change, differences in the cell area should be accompanied by opposite trends in their height. The same trend was obtained in terms of perimeter, yet with no significant differences.

Circularity and cell elongation factor (EF) were also calculated. Circularity is a quantitative parameter used to evaluate cell morphology, as well as cell EF. Significantly higher circularity values were obtained for flat CL $[CHT/CS]_{300}$, comparing with those obtained for PAT CL $[CHT/CS]_{300}$. These results indicate that fibroblasts grown on flat surfaces acquire more rounded morphologies than when grown in the nanopatterned surfaces, clearly consistent with the images of Figure 5A. Cell EF is defined as the ratio between the longest axis of the cell (length) and the longest axis perpendicular to it. Contrarily to area, perimeter and circularity, the EF of cells cultured on nanopatterned substrates was significant higher than for cell cultured above flat surfaces. As it was higher than 2 for PAT CL $[CHT/CS]_{300}$) it is possible to say that the majority of cells were elongated.[12]

Fibroblasts were cultured on substrates patterned with sub-micron wide stripes and, as already discussed, they elongated along the ridges and grooves direction. Flat substrates did not seem to have this ability. The angle between the topography direction and the longest axis of the cell was determined. Figure 5B shows the cell angle orientation distribution on flat CL $[CHT/CS]_{300}$ membranes, where the cell distribution seemed to be uniform in the range -90° to 90° and an indicative of a random orientation. On the other hand, as observed in Figure 5C, fibroblasts cultured on PAT CL $[CHT/CS]_{300}$ were distributed in the range -30° to 20° and approximately 71% of cells were aligned with the pattern direction (angle between -10° and 10°).[55] The phenomenon by which the matrix offers directional features to the cells and directs the motility response via anisotropy in the microenvironment has been designated as contact guidance.[4d, 56] This fact is based on the theory that cells make a projection in one direction depending on the shape and type of features it encountered; for nanopatterned surfaces, the alignment phenomenon will be expected in the direction with less topographic and mechanic obstruction.[57] The parameter that has been mostly correlated with cellular alignment are the groove depth, at sub-micro and nano-scales.[19, 58] The depth of the grooves should be smaller enough for cells run down into the grooves and form FAs and bigger enough for cells sense, with filapodia being able to adhere to the grooves and make cell aligning. Additionally, we also correlated the alignment of the cytoskeleton with the alignment of the nucleus and, in fact, they deformed in the same direction. This result is consistent with literature[59] that suggests that the cytoskeleton network mediates the nucleus deformation.

2.5 C2C12 cellular response

2.5.1 C2C12 morphology and FAs formation—C2C12 myoblasts were chosen to study the influence of topography in cell differentiation, since it is a well-known and characterized model that has been reported in literature to study the influence of surface distinct properties.[60] Proliferating mononucleated myoblasts differentiate and fuse to multinucleated myotubes. Prior to evaluate the C2C12 differentiation towards myotubes, the

morphology of the cells cultured above CL $[CHT/CS]_{300}$ and PAT CL $[CHT/CS]_{300}$ were investigated for 1, 3, 5 and 10 days of culture. Figure 6A shows the fluorescence microscopic images of C2C12 stained with phalloidin (cytoskeleton) and DAPI (nucleus). No significant differences in imaged cell density seem to exist between cells cultured above flat and nanopatterned surfaces. C2C12 adhered above CL $[CHT/CS]_{300}$ and PAT CL $[CHT/CS]_{300}$ presented well-organized F-actin on their cytoskeleton and spread on all over the surfaces with extended filapodia. The key of the influence of nanogrooved topography on myoblast morphology is related with the cellular alignment and the formed FAs. In the case of CL $[CHT/CS]_{300}$ membranes, the elongated myoblasts appeared to be random oriented on the surface, while, for the PAT CL $[CHT/CS]_{300}$ films, the elongated cells seemed to follow a specific orientation. In fact, the C2C12 cultured on nanopatterned surfaces seemed to be elongated within the nanotopography direction, starting from day one of culture. In day 3 and day 5 of culture, myoblasts were proliferative and started to form a C2C12 network; the cells extended their filapodia and started to communicate with neighboring cells. A higher cell density was imaged with 10 days of culture for both flat and patterned FS membranes.

SEM observations were also performed to follow up the morphology of C2C12 on the FS $[CHT/CS]_{300}$ membranes, during the first week of culture. Microscopic images reinforced the results of immunofluorescence with phalloidin and DAPI - see Figure 6B. Just with 4 hours of culture, myoblasts already started to elongate and acquired a spindle-shaped morphology, while for flat membranes they still remained with a round morphology. In day 3 of culture, both patterned and unpatterned surfaces presented elongated cells with EF higher than 1.4. CL $[CHT/CS]_{300}$ films presented random distributed and oriented cells but PAT CL $[CHT/CS]_{300}$ exhibited a better control of cellular distribution and orientation, with the filapodia extended mainly along the grooves direction. The patterned membranes induced cells fusion with a specific direction. Higher cellular densities were imaged for 7 days of culture and the alignment effect were maintained for the patterned surfaces. With increasing culture time, cells tended to elongate, with a decrease of the width and an increase of the length. These observations can be better understood by the formation of FA on the nanogrooved surface; as already reported in literature and discussed for L929, FAs were usually established on nanogrooved surfaces and they tend to extend protrusion in the direction without obstacles. The formation of FAs of the C2C12 adhered on flat and nanopatterned membranes were revealed using an immunofluorescent staining of vinculin after 3 and 5 days of culture - see Figure 6C. The influence of the patterning was also observed at the FAs level, in terms of orientation and morphology. For both time points the FAs seemed to be more distributed around the cells for flat CL $[CHT/CS]_{300}$, whereas for PAT CL $[CHT/CS]_{300}$ the FAs seemed confined in a preferential direction, supporting the idea of FAs are deeply involved in the mechanism of cellular alignment. Note that for 3 days of culture, the immunofluorescence with vinculin allowed to identify by staining the direction of the patterning and effectively a bigger part of FAs was constrained into the preferential direction of the topography.

2.5.2 Myogenic Differentiation—Troponin T was used as a marker for the expression of myogenic differentiation, in order to investigate the effect of the nanopatterns on

differentiation. To perceive this effect, two different media were tested for cell differentiation: DMEM supplemented with horse serum (DM), typically used to trigger the differentiation of C2C12 into myotubes, and DMEM medium supplemented with FBS (GM), used routinely as a growth medium. Figure 7 shows the results of the immunocytochemistry studies for 7 and 10 days of culture. The process of C2C12 differentiation comprises the fusion of myoblasts into multinucleated myotubes, expressing markers like troponin T.[61]

In the case of using DM, no significant differences on troponin T expression were observed between CL $[CHT/CS]_{300}$ and PAT CL $[CHT/CS]_{300}$ membranes. For 7 days of culture, myoblasts started to fuse and formed small myotubes; tissue culture polystyrene surfaces (TCPS) presented larger myotubes and this could be due to a faster differentiation process for plastic-treated substrates. At the 10^{th} day of culture, other myoblasts started to fuse with the small myotubes and longer and mature myotubes were formed. These observations are consistent with the basis of mammalian myoblast fusion, which occurs into two phases: an early phase of forming nascent myotubes and a later phase of forming mature myotubes.[62]

Contrarily, in the case of using GM, some differences were noted for unpatterned and patterned membranes. Visually, the amount of troponin T expression on the cells cultured on nanopatterned membranes using GM was considerably higher compared with flat membranes and TCPS; this can be a clear indication that when using a medium capable of inducing differentiation by itself, the pattern effect was almost masked. After 10 days of culture, myotubes were formed and presented a long and thin morphology; however, the cells reached a stage where they were overgrown. Myoblasts change their triangular shape to an elongated one during the early stages of differentiation;[63] this can support the results obtained in GM conditions. In the absence of DM, the presence of nanogrooved topography on PAT CL $[CHT/CS]_{300}$ prompted cells to acquired predominantly an elongated shape and could promote myoblast differentiation by itself with no need of special exogenous factors.

In Figure 7, it is also possible to perceive some indications of the effect of the nanogrooved topography, with myotubes oriented in a particular direction. The influence of topography on C2C12 differentiation was consistent with previous works.[60a, 64] In fact, the alignment step, which has been related with the cytoskeleton organization, has been suggested as a crucial process before cell fusion, and thus, an important step in differentiation;[64–65] actin filaments were randomly distributed in flat membranes while in nanopatterned ones a big part of actin filaments were aligned along the grooves. Moreover, by immunofluorescence images, morphological differences are perceived between flat CL $[CHT/CS]_{300}$ and PAT CL $[CHT/CS]_{300}$, using either DM or GM: for the flat ones myotubes presented an arc structure while for the nanogrooved surfaces they presented an aligned structure.

2.5.3 Morphometric parameters—The effect of the nanogrooves on myoblasts differentiation was also evaluated by exploring differentiation parameters: the fusion index, the number of troponin-positive myotubes, the area and the alignment of myotubes were determined for each condition after 10 days of culture.

Cells cultured on PAT CL $[CHT/CS]_{300}$ showed the highest percentage of fusion index, comparing with what happened with CL $[CHT/CS]_{300}$ - see Figure 8A. The fusion index percentage is significantly higher for PAT CL $[CHT/CS]_{300}$, either using DM or using GM. Otherwise, the number of troponin-positive myotubes is similar for flat CL $[CHT/CS]_{300}$ and PAT CL $[CHT/CS]_{300}$ when using DM, but significantly higher for PAT CL $[CHT/CS]_{300}$ in case of using GM. All these results together indicate that the myogenic differentiation into myotubes was boosted on PAT CL $[CHT/CS]_{300}$, mainly when using GM. Literature refers some different driving forces for myogenic differentiation but topography seemed to be one of the most significant.[66]

Either using DM or GM, significant differences in the myotubes area were found between flat and patterned FS films. The PAT CL $[CHT/CS]_{300}$ membranes presented myotubes with larger area than CL $[CHT/CS]_{300}$ - see Figure 8B. Regarding PAT CL $[CHT/CS]_{300}$ membranes, no significant differences were found in the myotubes area between DM or GM conditions.

Also myotubes alignment was evaluated for the different conditions, after 10 days of culture. Figure 8C displays the distribution of the myotubes orientation on the different membranes. For CL $[CHT/CS]_{300}$, using DM or GM, the myotubes were distributed in a wide range of orientations. On the other hand, for PAT CL $[CHT/CS]_{300}$ myotubes were distributed in a short range of orientation, presenting for both cases (DM or GM) a preferential orientation. These data are supported by related literature that described alignment as a driven force for myogenic differentiation.[67] In the present study, it is possible to correlate these 3 important concepts: a nanogrooved topography seemed to have an interesting impact on cellular alignment, which in turn promote myogenic differentiation even in absence of some special culture media.

3 Conclusion

Nanoengineered materials for biomedical applications have been showing remarkable advances in the last years. However, the complexity of the used methodologies and materials, the inability to create hierarchically organized and layered scaffolds, the time required and the short incorporation of non-meltable natural-based polymers have been the major obstacles in such developments. In this study, we developed a pioneer strategy to produce nanogrooved freestanding multilayer biopolymer films capable to control the cellular behavior. Using LbL methodology it was possible to process polysaccharide-based films with well-defined patterned motifs engraved on the surface with a sub-micrometer resolution. Cellular behavior was investigated for two different type of mammalian cells. For mouse fibroblasts, parameters like viability and proliferation had generally higher values on flat membranes and the nanotopography could induce significantly cell orientation. Moreover, also the alignment and myogenic differentiation of C2C12 were observed on nanopatterned membranes, even in absence of special differentiation medium. We were able to develop freestanding membranes using wet and mild processing routes, that depending on the post-processing steps (crosslinking) and the presence of topographic motifs could control cellular behavior, including orientation and differentiation without any external stimuli or exogenous factors. Such kind of versatile multilayer membranes could be valuable

bioinstructive substrates to be used in a variety of biomedical applications, such as in tissue engineering strategies.

Supplementary Material

Refer to Web version on PubMed Central for supplementary material.

Acknowledgements

Maria P. Sousa acknowledges the Portuguese Foundation for Science and Technology (FCT) for financial support through SFRH/BD/97606/2013 grant and Sofia G. Caridade through SFRH/BPD/96797/2013 grant.

References

[1]. a)Dalby MJ, Gadegaard N, Oreffo ROC. Nat Mater. 2014; 13:6.b)Kim D-H, Provenzano PP, Smith CL, Levchenko A. J Cell Biol. 2012; 197:3.

[2]. a)Kim HN, Jiao A, Hwang NS, Kim MS, Kang do H, Kim DH, Suh KY. Adv Drug Deliv Rev. 2013; 65:4.b)von der Mark K, Park J, Bauer S, Schmuki P. Cell Tissue Res. 2009; 339:1.

[3]. Weiner S, Wagner HD. Annu Rev Mater Sci. 1998; 28

[4]. a)Ventre M, Natale CF, Rianna C, Netti PA. J R Soc Interface. 2014; 11:100.b)Kehr NS, Riehemann K, El-Gindi J, Schäfer A, Fuchs H, Galla H-J, De Cola L. Adv Funct Mater. 2010; 20:14.c)Bettinger CJ, Zhang Z, Gerecht S, Borenstein JT, Langer R. Adv Mater. 2008; 20:1.d)Flemming RG, Murphy CJ, Abrams GA, Goodman SL, Nealey PF. Biomaterials. 1999; 20:6.

[5]. a) Khademhosseini, A, Ling, Y, Karp, JM, Langer, R. Micro- and Nanoscale Control of Cellular Environment for Tissue EngineeringNanobiotechnology II. Wiley-VCH Verlag GmbH & Co. KGaA; 2007. 347–364. b)Even-Ram S, Artym V, Yamada KM. Cell. 2006; 126:4.c)Wang DA, Williams CG, Yang F, Elisseeff JH. Adv Funct Mater. 2004; 14:12.

[6]. Chen W, Villa-Diaz LG, Sun Y, Weng S, Kim JK, Lam RHW, Han L, Fan R, Krebsbach PH, Fu J. ACS Nano. 2012; 6:5.

[7]. Yim EKF, Darling EM, Kulangara K, Guilak F, Leong KW. Biomaterials. 2010; 31:6.

[8]. Yim EK, Reano RM, Pang SW, Yee AF, Chen CS, Leong KW. Biomaterials. 2005; 26:26.

[9]. Kim DH, Kshitiz, Smith RR, Kim P, Ahn EH, Kim HN, Marban E, Suh KY, Levchenko A. Integr Biol. 2012; 4:9.

[10]. Lamers E, van Horssen R, te Riet J, van Delft FC, Luttge R, Walboomers XF, Jansen JA. Eur Cell Mater. 2010; 20

[11]. Kulangara K, Yang Y, Yang J, Leong KW. Biomaterials. 2012; 33:20. [PubMed: 21982297]

[12]. Teixeira AI, Abrams GA, Bertics PJ, Murphy CJ, Nealey PF. J Cell Sci. 2003; 116(Pt 10)

[13]. Teixeira AI, McKie GA, Foley JD, Bertics PJ, Nealey PF, Murphy CJ. Biomaterials. 2006; 27:21.

[14]. Kim J, Kim HN, Lim KT, Kim Y, Seonwoo H, Park SH, Lim HJ, Kim DH, Suh KY, Choung PH, Choung YH, et al. Sci Rep. 2013; 3

[15]. Dalby MJ, Riehle MO, Sutherland DS, Agheli H, Curtis AS. Biomaterials. 2004; 25:23. [PubMed: 14580905]

[16]. Dalby MJ, Riehle MO, Johnstone H, Affrossman S, Curtis ASG. Biomaterials. 2002; 23:14.

[17]. Smith LA, Ma PX. Colloids Surf, B. 2004; 39:3.

[18]. Norman JJ, Desai TA. Ann Biomed Eng. 2006; 34:1.

[19]. Loesberg WA, te Riet J, van Delft FCMJM, Schön P, Figdor CG, Speller S, van Loon JJWA, Walboomers XF, Jansen JA. Biomaterials. 2007; 28:27.

[20]. a)Costa RR, Mano JF. Chem Soc Rev. 2014; 43:10.b)Decher G. Science. 1997; 277:5330.

[21]. a)Niepel MS, Mano JF, Groth T. ACS Appl Mater Interfaces. 2016; 8:38.b)Monge C, Saha N, Boudou T, Pózos-Vásquez C, Dulong V, Glinel K, Picart C. Advanced Functional Materials. 2013; 23:27.

[22]. Caridade SG, Monge C, Gilde F, Boudou T, Mano JF, Picart C. Biomacromolecules. 2013; 14:5.

[23]. Zhang J, Senger B, Vautier D, Picart C, Schaaf P, Voegel J-C, Lavalle P. Biomaterials. 2005; 26:16.

[24]. Wittmer CR, Phelps JA, Saltzman WM, Van Tassel PR. Biomaterials. 2007; 28:5.

[25]. Ye X, Wang H, Zhou J, Li H, Liu J, Wang Z, Chen A, Zhao Q. PLoS ONE. 2013; 8:1.

[26]. Boudou T, Crouzier T, Ren K, Blin G, Picart C. Adv Mater. 2010; 22:4.

[27]. Correia CR, Reis RL, Mano JF. Biomacromolecules. 2013; 14:3.

[28]. a)Alves NM, Picart C, Mano JF. Macromolecular Bioscience. 2009; 9:8.b)Höök F, Kasemo B, Nylander T, Fant C, Sott K, Elwing H. Anal Chem. 2001; 73:24.

[29]. Anene-Nzelu CG, Choudhury D, Li H, Fraiszudeen A, Peh K-Y, Toh Y-C, Ng SH, Leo HL, Yu H. Biomaterials. 2013; 34:21.

[30]. Marco C, Giorgia B, Michela S, Fabio B. Nanotechnology. 2007; 18:50.

[31]. Cecchini M, Ferrari A, Beltram F. JPCS. 2008; 100:1.

[32]. Wang P-Y, Yu J, Lin J-H, Tsai W-B. Acta Biomater. 2011; 7:9.

[33]. Sousa MP, Cleymand F, Mano JF. Biomed Mater. 2016; 11:3.

[34]. Oliveira SM, Alves NM, Mano JF. J Adhes Sci Technol. 2014; 28:8–9.

[35]. a)Chen H, Ouyang W, Lawuyi B, Prakash S. Biomacromolecules. 2006; 7:7.b)Mi F-L, Sung H-W, Shyu S-S. J Polym Sci A Polym Chem. 2000; 38:15.

[36]. Gao L, Gan H, Meng Z, Gu R, Wu Z, Zhang L, Zhu X, Sun W, Li J, Zheng Y, Dou G. Colloids Surf, B. 2014; 117

[37]. Silva JM, Caridade SG, Oliveira NM, Reis RL, Mano JF. J Mater Chem B. 2015; 3:22.

[38]. Cassie ABD, Baxter S. Trans Faraday Soc. 1944; 40

[39]. Kehr NS, Motealleh A, Schäfer AH. ACS Appl Mater Interfaces. 2016; 8:51.

[40]. a)Engler AJ, Sen S, Sweeney HL, Discher DE. Cell. 2006; 126:4.b)Saha K, Keung AJ, Irwin EF, Li Y, Little L, Schaffer DV, Healy KE. Biophys J. 2008; 95:9.

[41]. a)Caridade SG, Monge C, Almodovar J, Guillot R, Lavaud J, Josserand V, Coll JL, Mano JF, Picart C. Acta Biomater. 2015; 15b)Mano JF. Macromol Biosci. 2008; 8:1.

[42]. Silva JM, Duarte ARC, Caridade SG, Picart C, Reis RL, Mano JF. Biomacromolecules. 2014; 15:10.

[43]. Alves NM, Gómez R, Gómez T, Mano JF. Macromolecules. 2004; 37:10.

[44]. Azevedo, HS, Reis, RL. Understanding the enzymatic degradation of biodegradable polymers and strategies to control their degradation rateBiodegradable systems in tissue engineering and regenerative medicine. CRC Press; 2005. 177–201.

[45]. Nordtveit RJ, Vårum KM, Smidsrød O. Carbohydr Polym. 1996; 29:2.

[46]. Honda T, Kaneiwa T, Mizumoto S, Sugahara K, Yamada S. Biomolecules. 2012; 2:4.

[47]. a)Cardoso MJ, Caridade SG, Costa RR, Mano JF. Biomacromolecules. 2016; 17:4. [PubMed: 26607961] b)Aurore S, Ludovic R, Gregory F, Jean-Claude V, Catherine P. Biomed Mater. 2007; 2:1. [PubMed: 18458426]

[48]. a)Yan LP, Wang YJ, Ren L, Wu G, Caridade SG, Fan JB, Wang LY, Ji PH, Oliveira JM, Oliveira JT, Mano JF, et al. J Biomed Mater Res A. 2010; 95:2.b)Etienne O, Schneider A, Taddei C, Richert L, Schaaf P, Voegel JC, Egles C, Picart C. Biomacromolecules. 2005; 6:2.

[49]. a)Kim D-H, Han K, Gupta K, Kwon KW, Suh K-Y, Levchenko A. Biomaterials. 2009; 30:29.b)Rebollar E, Frischauf I, Olbrich M, Peterbauer T, Hering S, Preiner J, Hinterdorfer P, Romanin C, Heitz J. Biomaterials. 2008; 29:12.

[50]. Miller DC, Thapa A, Haberstroh KM, Webster TJ. Biomaterials. 2004; 25:1. [PubMed: 14580903]

[51]. Neto AI, Vasconcelos NL, Oliveira SM, Ruiz-Molina D, Mano JF. Adv Funct Mater. 2016; 26:16.

[52]. a)Choi CH, Hagvall SH, Wu BM, Dunn JC, Beygui RE, CJK CJ. Biomaterials. 2007; 28:9. [PubMed: 16952394] b)Wood MA, Wilkinson CD, Curtis AS. IEEE Trans Nanobioscience. 2006; 5:1. [PubMed: 16570867] c)Berry CC, Dalby MJ, McCloy D, Affrossman S. Biomaterials. 2005; 26:24.d)Dalby MJ, Riehle MO, Sutherland DS, Agheli H, Curtis ASG. Biomaterials. 2004;

25:23. [PubMed: 14580905] e)Dalby MJ, Riehle MO, Johnstone HJ, Affrossman S, Curtis AS. Tissue Eng. 2002; 8:6.

[53]. Fujita S, Ohshima M, Iwata H. Journal of the Royal Society, Interface / the Royal Society. 2009; 6(Suppl 3)

[54]. Versaevel M, Grevesse T, Gabriele S. Nat Commun. 2012; 3:671. [PubMed: 22334074]

[55]. Clark P, Connolly P, Curtis AS, Dow JA, Wilkinson CD. Development. 1990; 108:4.

[56]. Curtis A, Wilkinson C. Biomaterials. 1997; 18:24.

[57]. Alapan Y, Younesi M, Akkus O, Gurkan UA. Adv Healthc Mater. 2016; 5:15.

[58]. a)Fraser SA, Ting Y-H, Mallon KS, Wendt AE, Murphy CJ, Nealey PF. Journal of biomedical materials research Part A. 2008; 86:3.b)Walboomers XF, Croes HJE, Ginsel LA, Jansen JA. J Biomed Mater Res. 1999; 47:2.

[59]. Nathan AS, Baker BM, Nerurkar NL, Mauck RL. Acta Biomater. 2011; 7:1. [PubMed: 20619368]

[60]. a)Padmanabhan J, Augelli MJ, Cheung B, Kinser ER, Cleary B, Kumar P, Wang R, Sawyer AJ, Li R, Schwarz UD, Schroers J, et al. Scientific Reports. 2016; 6b)Cantini M, Sousa M, Moratal D, Mano JF, Salmeron-Sanchez M. Biomater Sci. 2013; 1:2.

[61]. Cabane C, Englaro W, Yeow K, Ragno M, Dérijard B. Am J Physiol Cell Physiol. 2003; 284:3.

[62]. Horsley V, Pavlath GK. Cells Tissues Organs. 2004; 176:1–3.

[63]. a)Ku SH, Park CB. Biomaterials. 2013; 34:8.b)Swailes NT, Colegrave M, Knight PJ, Peckham M. J Cell Sci. 2006; 119(Pt 17)

[64]. a)Yang HS, Lee B, Tsui JH, Macadangdang J, Jang SY, Im SG, Kim DH. Adv Healthc Mater. 2016; 5:1.b)Cooper A, Jana S, Bhattarai N, Zhang M. Journal of Materials Chemistry. 2010; 20:40.

[65]. Aubin H, Nichol JW, Hutson CB, Bae H, Sieminski AL, Cropek DM, Akhyari P, Khademhosseini A. Biomaterials. 2010; 31:27.

[66]. Dang JM, Leong KW. Adv Mater. 2007; 19:19.

[67]. Ostrovidov S, Hosseini V, Ahadian S, Fujie T, Parthiban SP, Ramalingam M, Bae H, Kaji H, Khademhosseini A. Tissue Eng Part B Rev. 2013; 20:5.

Europe PMC Funders Author Manuscripts

Europe PMC Funders Author Manuscripts

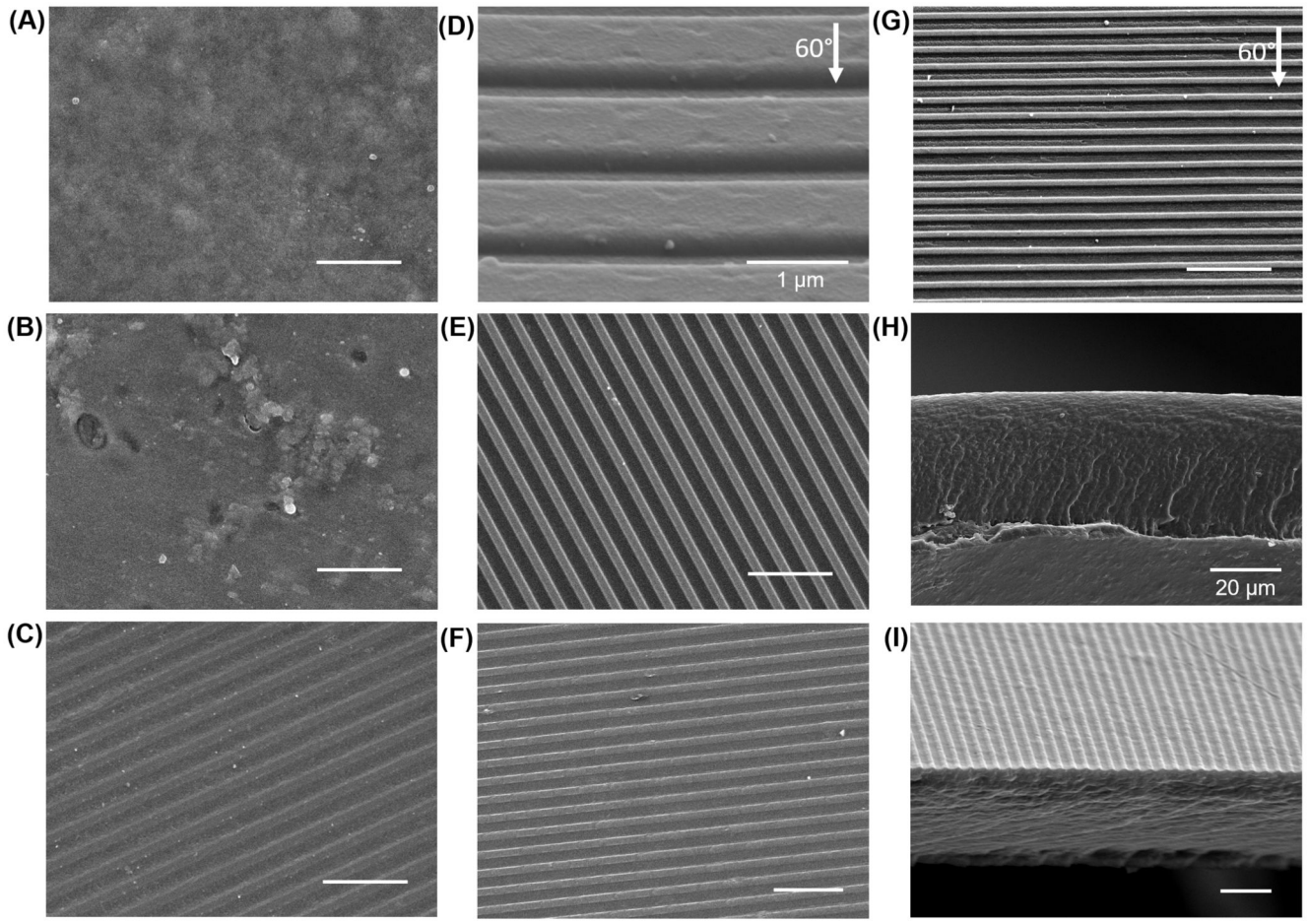

Figure 1.

Representative SEM images of A) $[CHT/CS]_{300}$, B) CL $[CHT/CS]_{300}$, C) top-view and D) tilted view (60°) of optical media used as template to produce the patterned (PAT) membranes, E) PAT $[CHT/CS]_{300}$, F) PAT CL $[CHT/CS]_{300}$ and G) PAT CL $[CHT/CS]_{300}$ tilted at 60°. SEM images of the cross-sections of H) $[CHT/CS]_{300}$ and I) PAT $[CHT/CS]_{300}$ membranes. The scale bars represent 5 μm unless for the image where it appears with the value.

Europe PMC Funders Author Manuscripts

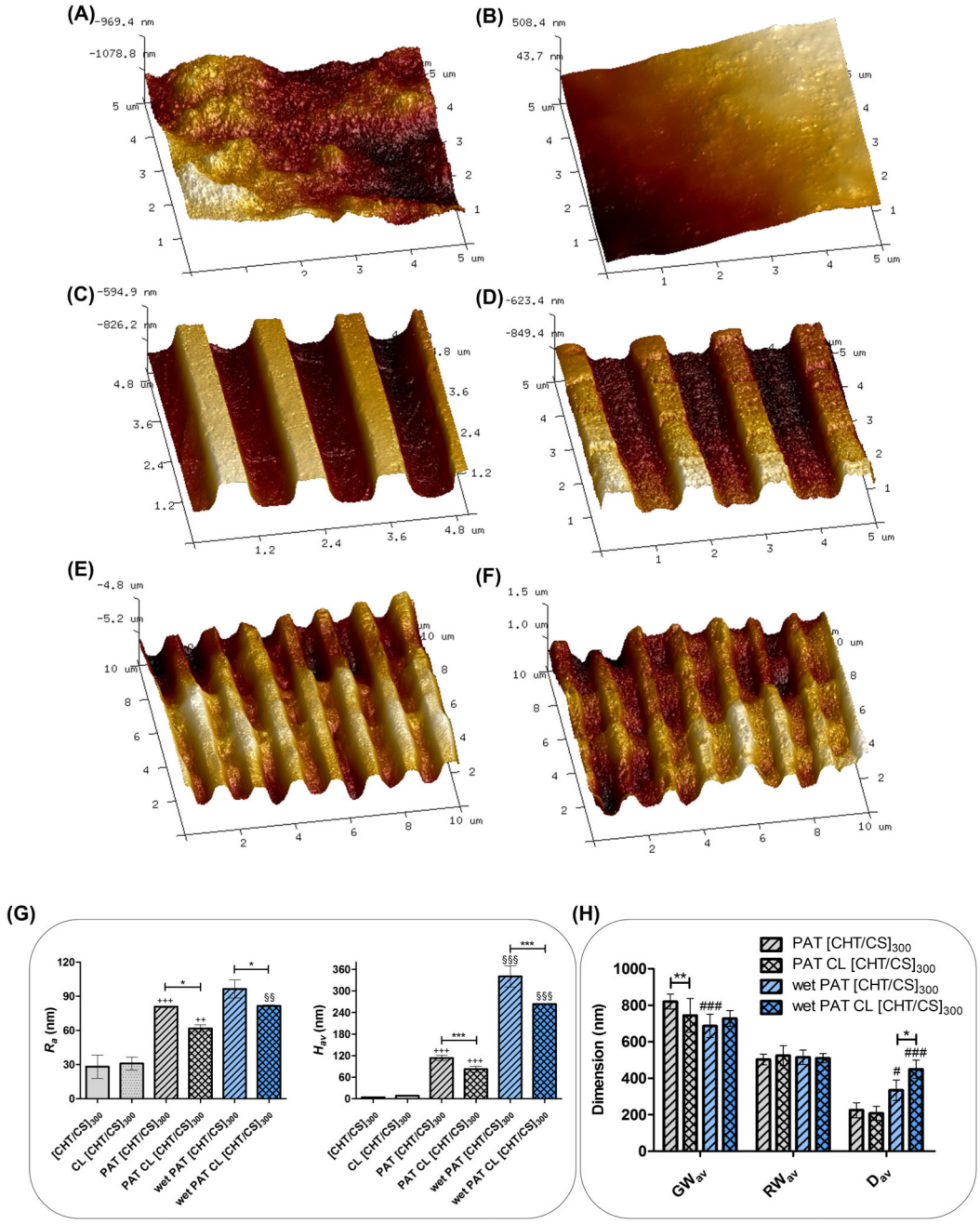

Figure 2.

Representative AFM images of A) $[CHT/CS]_{300}$, B) CL $[CHT/CS]_{300}$, C) PAT $[CHT/CS]_{300}$, D) PAT CL $[CHT/CS]_{300}$ topographies in air, E) PAT $[CHT/CS]_{300}$ and F) PAT CL $[CHT/CS]_{300}$ in fluid. G) Arithmetic roughness (R_a) and average height value (H_{av}) for flat and patterned surfaces. H) Averaged dimensions of the nanofeatures, with the values for groove (GW_{av}) and ridge (RW_{av}) widths and the depth (D_{av}) for the different membranes in both dry (air) or wet (PBS) states. Significant differences for the patterning effect were found for (++) $p<0.01$ and (+++) $p<0.001$ and for the crosslink effect were found for (*)

p<0.01 and (***) p<0.001. Significant differences between dry and wet states were found for (§§) p<0.01 and (§§§) p<0.001.

Europe PMC Funders Author Manuscripts

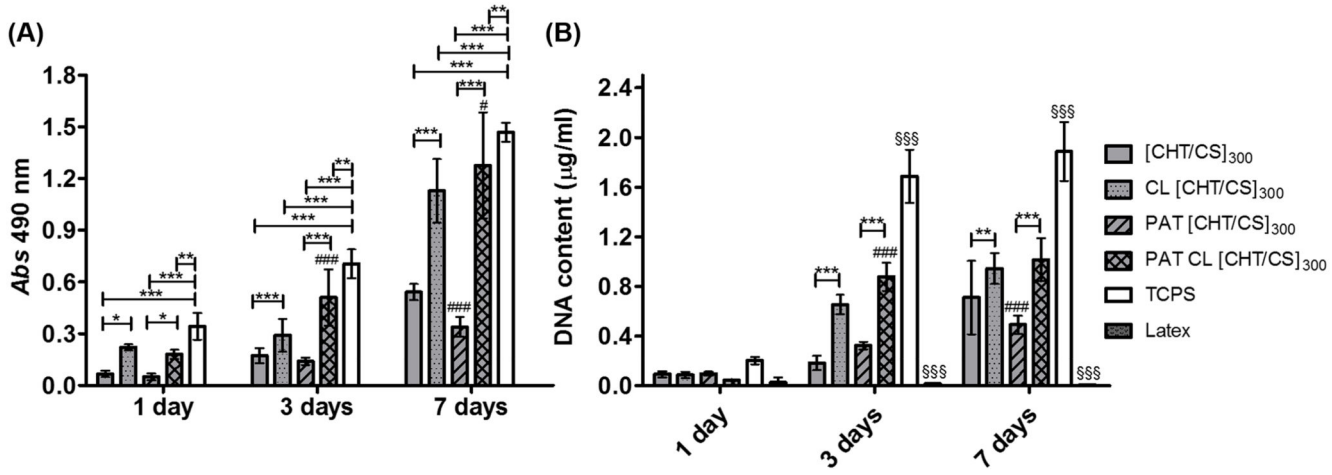

Figure 3.

A) cellular viability through the absorbance of the metabolic activity of L929 cells (MTS assay) in function of culturing time and B) cellular proliferation through the determination of the DNA content (DNA quantification assay) in function of culturing time. Significant differences for the crosslink effect were found for (***) $p < 0.001$, (**) $p < 0.01$ and (*) $p < 0.05$. Significant differences for the patterning effect were found for (###) $p<0.001$ and (#) $p<0.05$. Significant differences were found for (***) $p < 0.001$ and (**) $p < 0.01$ with TCPS and for (§§§) $p < 0.001$ with latex.

Europe PMC Funders Author Manuscripts

Europe PMC Funders Author Manuscripts

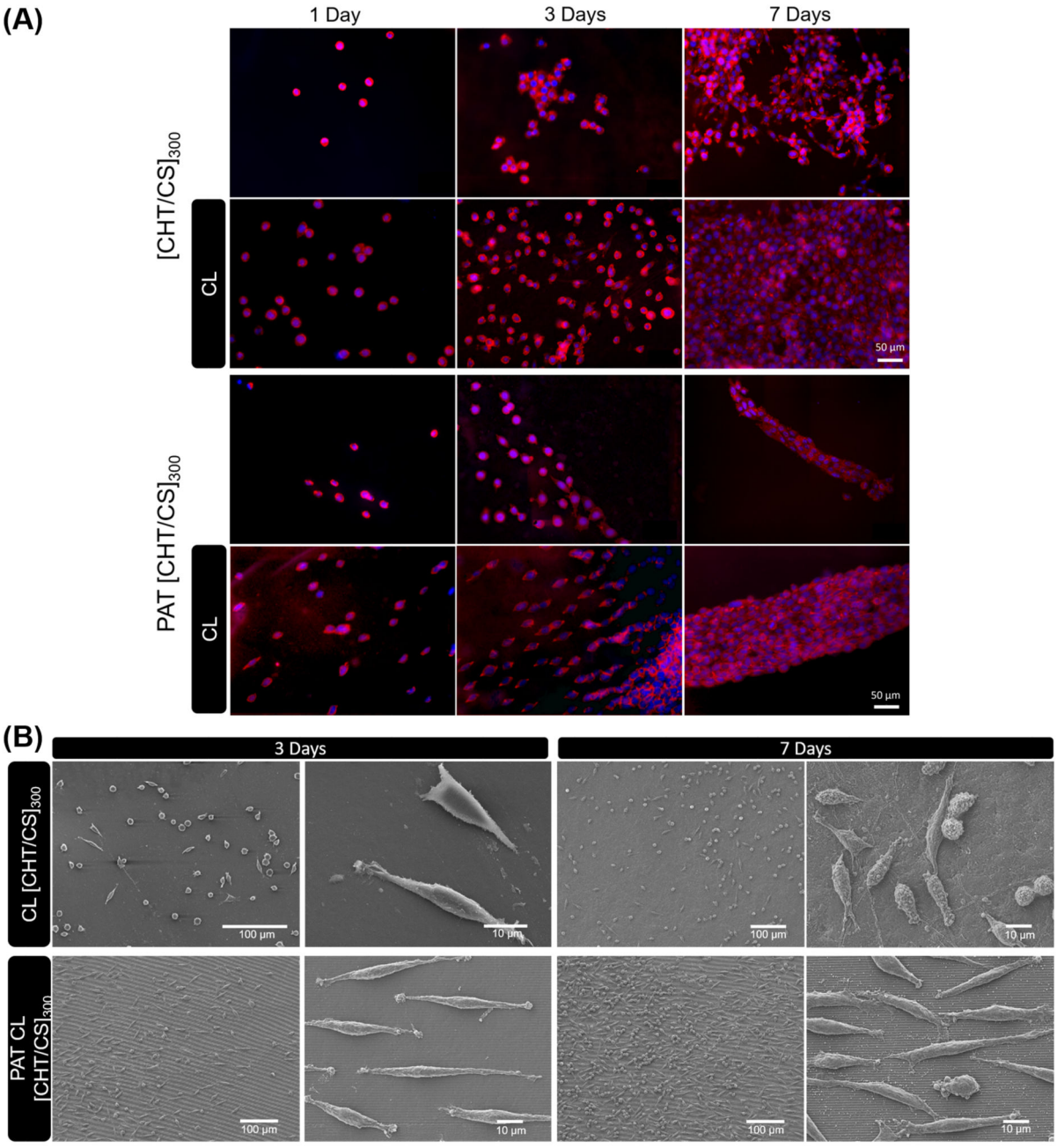

Figure 4.

Representative images of L929 cells over the different membranes. (A) DAPI−phalloidin fluorescence assay at 1, 3 and 7 days of culture on flat and nanopatterned $[CHT/CS]_{300}$ membranes, with or without crosslinking. Cells nuclei are stained in blue by DAPI and F-actin filaments are stained in red by phalloidin. The scale bar is representative for all images. B) SEM observation at 3 and 7 days of culture above crosslinked flat and nanopatterned CL $[CHT/CS]_{300}$ membranes.

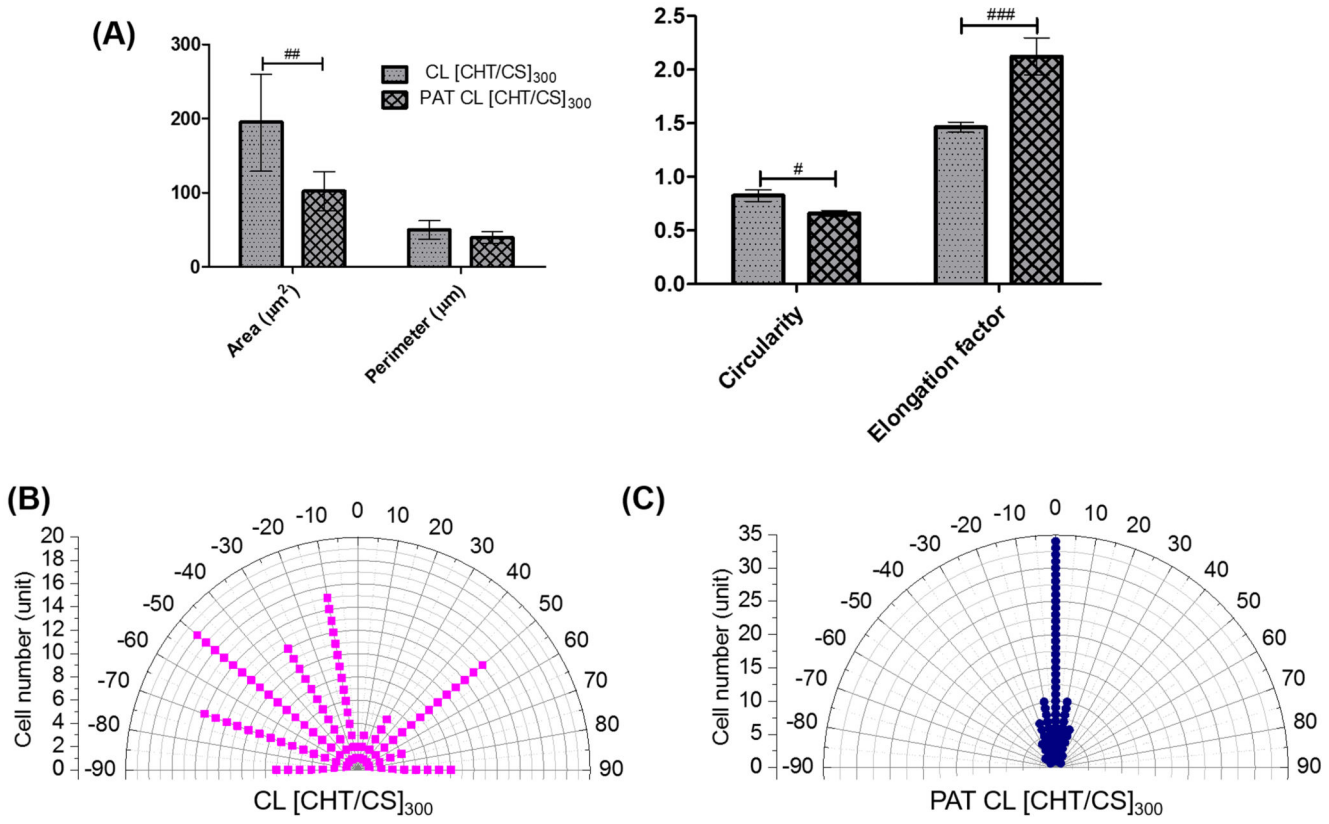

Figure 5.

Morphometric parameters of L929 cell adhered on crosslinked flat and nanopatterned membranes: A) cell area, perimeter, circularity and elongation factor (EF). Polar graphical representation of cellular alignment for B) CL $[CHT/CS]_{300}$ and for C) PAT CL $[CHT/CS]_{300}$. For each parameter, significant differences were found for (#) $p < 0.05$, (##) $p < 0.01$ and for (###) $p < 0.001$.

Europe PMC Funders Author Manuscripts

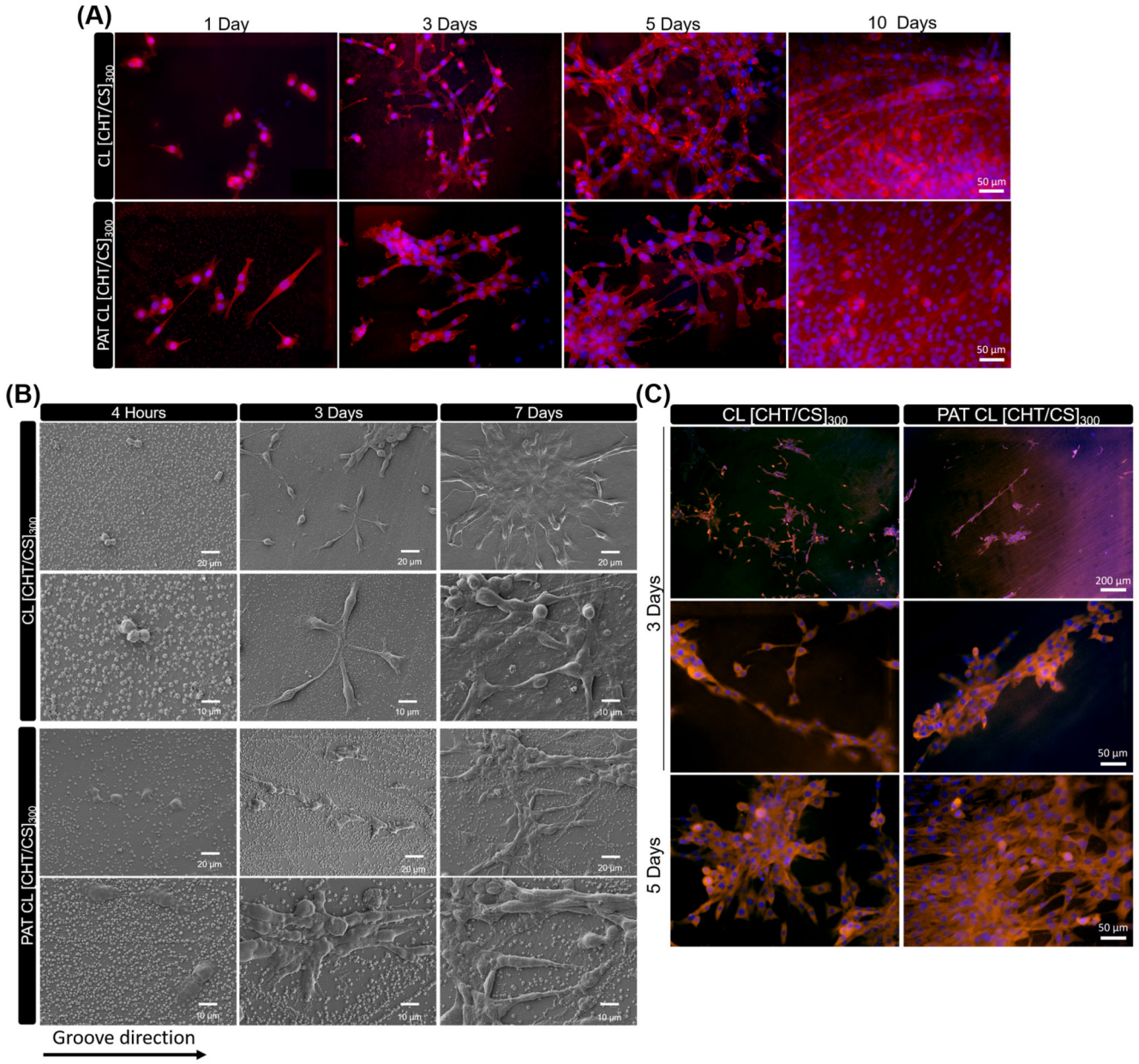

Figure 6.

Representative images of C2C12 cells over the different CL membranes. (A) DAPI −phalloidin fluorescence assay at 1, 3, 5 and 10 days. Cells nuclei are stained in blue by DAPI and F-actin filaments are stained in red by phalloidin. The scale bar is representative for all images. B) SEM observation at 4 hours, 3 and 7 days, at different magnifications and C) Immunofluorescence with vinculin (orange focal adhesions) and DAPI (blue nuclei) at 3 and 5 days. The scale bar is representative for all images, at different magnifications. Images are representative of CL flat and nanopatterned $[CHT/CS]_{300}$ membranes.

Europe PMC Funders Author Manuscripts

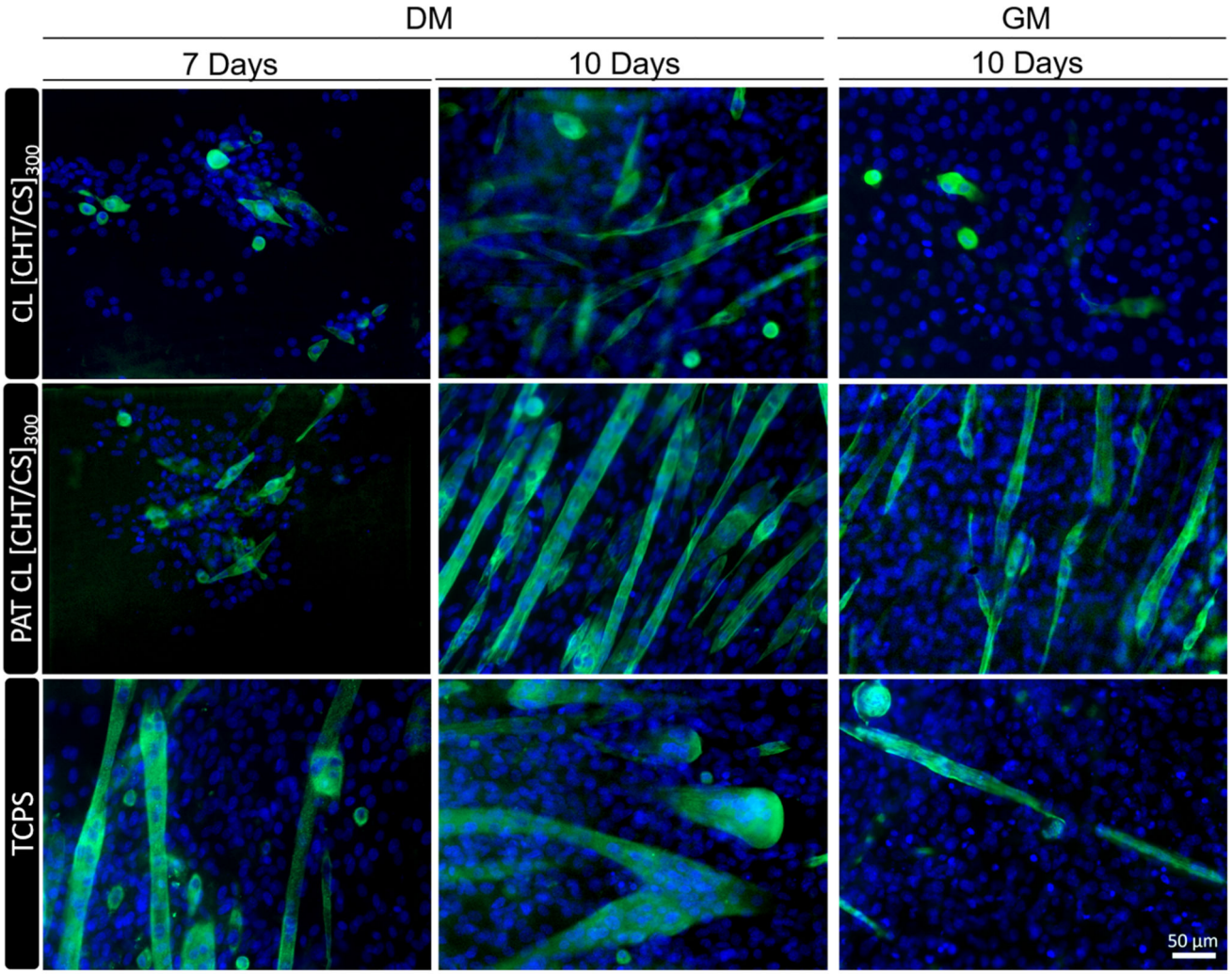

Figure 7.

Immunofluorescence with troponin T (green myotubes) and DAPI (blue nuclei) at 7 and 10 days of culture. Images are representative of crosslinked flat and nanopatterned CHT/CS membranes and TCPS, using differentiation medium (DM) and normal growth medium (GM). The scale bar is representative for all images.

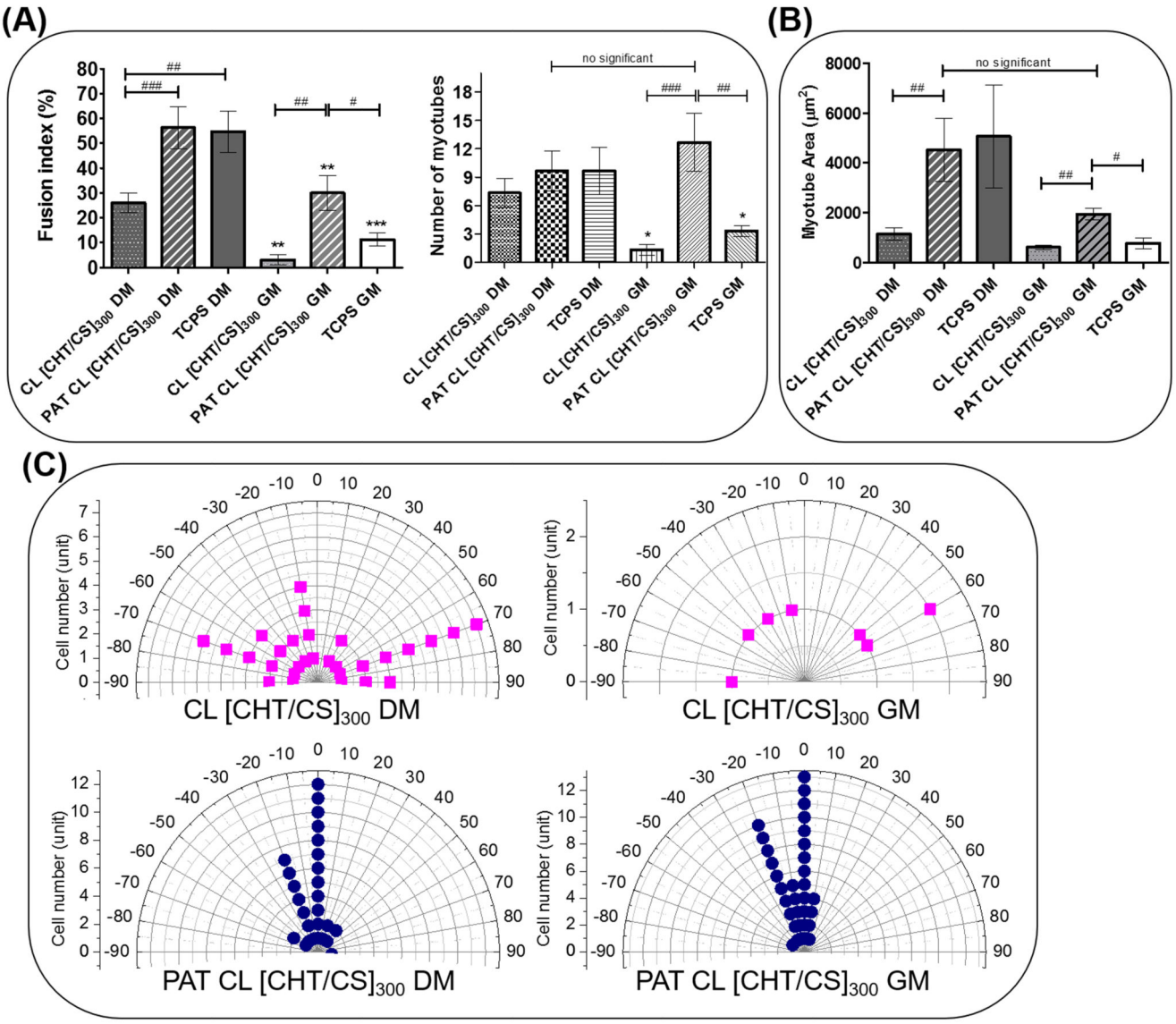

Figure 8.

Morphometric parameters of C2C12 cell adhered on crosslinked flat and nanopatterned membranes: A) fusion index (%) and normalized number of myotubes and B) myotube area in an established area. For the effect of the culture medium, significant differences were found for (***) $p < 0.001$ and (**) $p < 0.01$ and for patterning effect the significant differences were found for (#) $p < 0.05$, (##) $p < 0.01$ and (###) $p < 0.001$. The statistical analysis for myotube area parameter was done using a nonparametric equivalent of one-way ANOVA (Kruskal–Wallis test) followed by Dunn's multiple comparison test. C) Polar graphical representation of cellular alignment for CL $[CHT/CS]_{300}$ and for PAT CL $[CHT/CS]_{300}$. It is assumed that the preferential alignment corresponds to the grooves orientation (arbitrary angle).